DUAL-FREQUENCY VLA OBSERVATIONS OF THE EXTENDED RADIO GALAXY 3C 166

STEVEN R. SPANGLER AND ALAN H. BRIDLE[a]
National Radio Astronomy Observatory,[b] Socorro, New Mexico 87801
Received 13 April 1982; revised 24 May 1982

ABSTRACT

We have observed the radio galaxy 3C 166 at 1.4 and 4.9 GHz using the "A" and "B" configurations of the Very Large Array to provide an angular resolution of 1.6″ at both frequencies. The source has a basically double structure with strikingly dissimilar lobes. The south lobe is brightened along its outer edge, with a prominent hot spot, whereas the north lobe is relaxed in appearance with more feeble interior brightness maxima. The south lobe is strongly Faraday depolarized at 1.4 and possibly also at 4.9 GHz, but there is no measurable Faraday depth in the north lobe. The results are used to estimate magnetic field strengths and thermal particle densities in the lobes.

I. INTRODUCTION

With the completion of the NRAO Very Large Array (VLA), it has become possible to make observations at several frequencies with very similar (u, v) plane coverages. The completed VLA (Thompson *et al.* 1981; Heeschen 1981) can be configured in any of four homologous arrays, the largest three of which have sizes nearly scaling with the standard observing wavelengths of 20, 6, and 2 cm. Thus, in the "A array," characterized by a longest baseline of 35 km, observations at 20 cm have baseline lengths in wavelengths which are nearly identical to those of 6-cm observations in the "B array," in which the longest baseline is about 11 km. Using this, one can measure the frequency dependence of total intensity and polarization distributions across extended sources without introducing uncertainties due to unequal sensitivities to different structural scales at different frequencies.

This paper presents 1.4- and 4.9-GHz observations of the extended structure of the radio galaxy 3C 166. We observed 3C 166 for two reasons. Spangler and Cook (1980) had previously observed 15 steep-spectrum sources reported as variable at 2.7 GHz by Kesteven, Bridle, and Brandie (1976). Their "snapshot" map of 3C 166 appeared to show a symmetric jet emanating from an unresolved central component; presumably this unresolved component is responsible for the variability observed by Kesteven, Bridle, and Brandie. We therefore reobserved 3C 166 (a) to examine the variability of this central component directly, and (b) to obtain better maps of its extended structure. This paper concentrates on the properties of the extended emission; the variability of the central component will be discussed elsewhere.

The source has been identified with a $m_V = 17.7$ galaxy (Bridle and Fomalont 1978) of redshift 0.246 (Burbidge and Crowne 1979). It is in a cluster of galaxies (Wyndham 1966).

II. OBSERVATIONS AND DATA REDUCTION

The 1.4-GHz observations in the "A array" were made in January 1981, and the "B array" observations at 4.9 GHz in June 1981. The IF bandwidths were 25 MHz at 1.4 GHz and 50 MHz at 4.9 GHz; the small degradation of sensitivity away from the field center due to the finite bandwidth is therefore similar at the two observing frequencies. At both frequencies, 3C 166 was observed around 2^h from transit for about two hours, exclusive of time spent for calibration observations, etc.

In calibrating the data, we exploited the fact that 3C 166 contains a strong, flat-spectrum central component which is unresolved to the VLA (see Figs. 1 and 2). The flux density of this central component was calibrated relative to flux densities of 1.56 Jy for the source 0528+134 at 1.4 GHz and 2.27 Jy for the source 0735+178 at 4.9 GHz. These were measured relative to assumed flux densities on the Baars *et al.* (1977) scale of 8.7 and 4.2 Jy for 3C 138 at 1.4 and 4.9 GHz and of 7.41 Jy for 3C 286 at 4.9 GHz. The comparison with 3C 138 was made using only the inner 50 000 λ of the array, as 3C 138 is significantly resolved at longer baselines.

Instrumental and atmospheric gain and phase fluctuations were monitored using the data on long baselines over which the extended structure was resolved out, so that only the unresolved central component contributed significantly to the observed visibility. This technique uses the core component as a phase reference to monitor atmospheric fluctuations along the line of sight to the source at the time of the observations, rather than relying on asynchronous measurements of external calibration sources which may be several degrees away. This allows us to update the effective complex gains of the antennas rapidly enough to follow and remove atmospheric phase fluctuations, and thus to optimize the dynamic range of the images of the extended structure.

The calibrated data were mapped in the usual way and CLEANed (Hogbom 1974) using the procedure de-

[a] On leave from Queen's University at Kingston, Ontario K7L 3N6, Canada.

[b] The National Radio Astronomy Observatory is operated by Associated Universities, Inc., under contract from the National Science Foundation.

 0004-6256/82/091270-09$00.90

veloped by Clark (1980). The mapping and subsequent image manipulation were carried out with the NRAO Astronomical Image Processing System (AIPS) developed by E. B. Fomalont and colleagues.

Trials of several tapers in the (u, v) plane resulted in a choice of a Gaussian function falling to 0.30 at 120 000 λ as an attractive compromise between resolution and sensitivity to low surface brightness features. The total intensity (Stokes parameter I) maps were CLEANed until the sum of the CLEAN component flux densities converged. At this point the residual maps were compatible with the expected system noise and the sum of the CLEAN components was consistent with both the known single-dish flux densities for 3C 166 and the maximum amplitudes of the observed visibility functions at short baselines. The magnitude of the total-intensity variations observed in 3C 166 at 2.7 GHz is only 0.15 Jy (Kesteven, Bridle, and Brandie 1976), so the comparison with the catalogued single-dish flux densities is meaningful.

The polarized (Stokes parameters Q and U) maps were CLEANed until the total flux density in CLEANed components had converged and the residual map was consistent with the expected radiometer noise level. These precautions are essential so that all features on the CLEANed maps are observed at the same effective resolution, i.e., that of the restoring beam (which was a circular Gaussian of FWHM 1.6″).

Table I summarizes the map characteristics. Column 1 gives the observing frequency and column 2 lists the Stokes parameter of the map. Column 3 lists the total flux density in the CLEANed components. Finally, column 4 gives the fluctuation level on the map (in mJy per beam area), determined in a region of the CLEANed map far from the source.

It should be noted that the rms fluctuation values given in Table I represent the map characteristics away from the source and are determined by radiometer noise (for the Q and U maps) and also by finite dynamic range (for the I maps). They are not necessarily good estimates of the errors of observation in the source, which may be larger.

III. OBSERVATIONAL RESULTS

a) Total intensity

Figures 1 and 2 show that 3C 166 has a strong unresolved central core component and two resolved lobes.

TABLE I. Map characteristics.

Freq. (GHz)	Pol.	S_{tot} (mJy)	rms fluctuation (mJy/beam)
1.413	I	2450	0.56
	Q	− 28	0.12
	U	2.2	0.16
4.885	I	840	0.23
	Q	− 4.2	0.093
	U	− 7.1	0.087

A loop gain of 0.20 was used in all CLEANs.

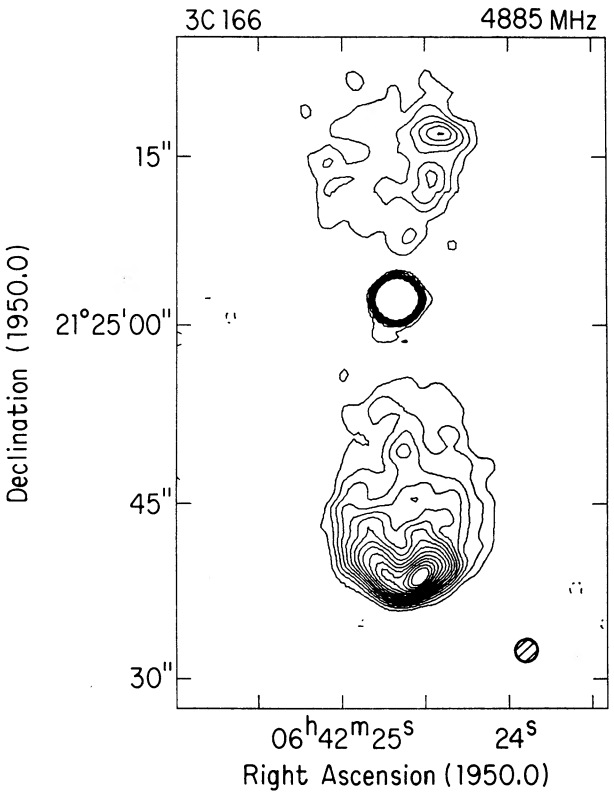

FIG. 1. Total intensity map at 4.885 GHz. There are 15 evenly spaced contours beginning at 0.25% of the peak intensity, which is 0.437 Jy/beam. The restoring beam is 1.6″ FWHM, shown as the cross-hatched circle.

The south lobe is more luminous than the north, and has a bright rim and hot spot at its outer edge. The north lobe, in contrast, has a diffuse, "relaxed" appearance, with two feeble brightness maxima in its interior. For an object with the redshift of 3C 166 ($z = 0.246$) and an assumed Hubble constant of $H_0 = 100$ km s^{-1} Mpc^{-1}, the image scale is 2.5 kpc arcsec^{-1}. The overall size of the source is therefore $\simeq$115 kpc.

Figures 1 and 2 show that the central extended emission is wider in the direction perpendicular to the source axis than was indicated by the lower dynamic range map of Spangler and Cook (1980). The categorization of this emission as a jet now seems inappropriate, and the structure would be better described as an elongated lobe or extended radio bridge. The new VLA observations indicate that, at the very least, 3C 166 does not possess a well defined jet of the type frequently found in low-luminosity radio galaxies (e.g., Bridle 1981; Fanti and Parma 1981; Ekers *et al.* 1981).

b) Polarized Intensity

The maps of polarized intensity $(Q^2 + U^2)^{1/2}$ shown in Figs. 3 and 4 reveal a pronounced frequency dependence of the polarized structure. The polarized structure of the north lobe is essentially the same at both observing frequencies, but that of the south lobe is mar-

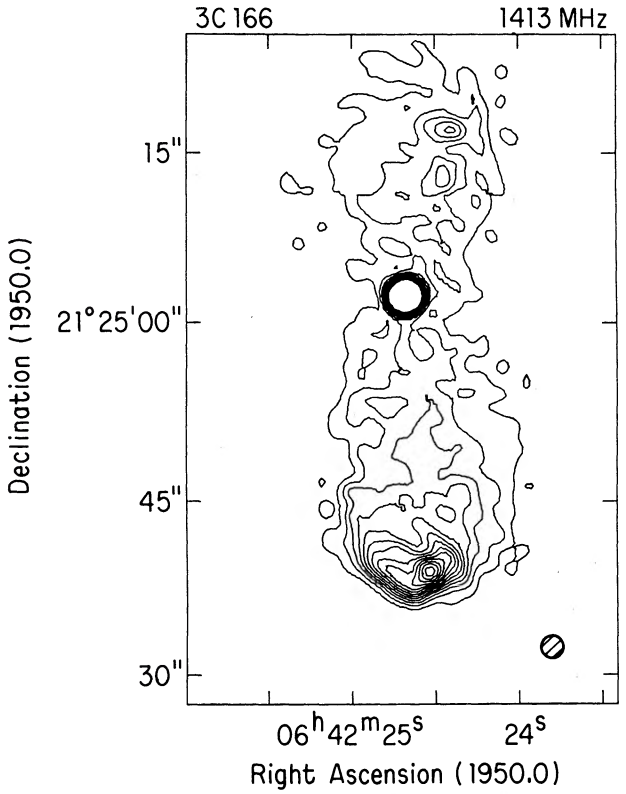

FIG. 2. Total intensity map at 1.413 GHz. There are 15 evenly spaced contours beginning at 1% of the peak intensity, which is 0.376 Jy/beam. The restoring beam is 1.6" FWHM, shown as the cross-hatched circle.

kedly different at the two frequencies. At 4.9 GHz (Fig. 3) much of the south lobe is significantly polarized. In particular, the prominent hot spot (feature *A* in Fig. 3) and its associated ridge (feature *B*) are 10%–20% polarized. Two features in the interior of the lobe (features *C* and *D*) are also 20%–50% polarized at this frequency. There is little polarized emission between the outermost part of the rim and these interior features, however. At 1.4 GHz (Fig. 4), only feature *D* remains strongly polarized; its fractional linear polarization at this frequency is $\simeq$35%, comparable to that at 4.9 GHz ($\simeq$50%). The fractional polarization of the hot spot (feature *A*) is only about 2%, much less than at 4.9 GHz.

Figures 5 and 6 show the orientation of the electric field vectors at the two frequencies. Before discussing these data, we consider the possible effect of galactic Faraday rotation, in view of the low galactic latitude of 3C 166 ($b_{II} = 8$ deg). The rotation measure (RM) maps of Simard-Normandin and Kronberg (1980) show that the average RM of extragalactic sources in this area of the sky is of order 30–45 rad m^{-2}. Such a rotation measure would result in 4.9-GHz position angles which were 6–9 deg from intrinsic. The difference between the 4.9- and 1.4-GHz position angles due to this foreground Faraday rotation would be 70–106 deg. A position angle difference map, constructed by subtracting the position angles in Fig. 5 from those in Fig. 6, showed that regions of the source for which the depolarization data indicate small internal Faraday depths (feature *D* and portions of the north lobe) are characterized by very small rotations of the polarization position angles (of order a few degrees) between 1.4 and 4.9 GHz. The simplest explanation of this observation is that 3C 166 lies in a direction of anomalously small galactic Faraday rotation (relative to the general pattern indicated by Simard-Normandin and Kronberg). In any case, the 4.9-GHz electric vectors for 3C 166 should be within $\simeq$10 deg of the intrinsic (zero-wavelength) orientations.

c) Magnetic Structure of the Lobes

Given the low RM, Fig. 5 shows that the magnetic field is circumferential around the southeast rim of the south lobe. This may be a general property of the lobes of luminous radio galaxies (Dreher 1981). In the feature marked *D* on Fig. 3, the magnetic field is perpendicular to the source axis. In feature *C*, the field appears to be parallel to the axis, but the observed depolarization indicates that this emission has traversed a large Faraday depth in the source, so the true field direction here is uncertain. The field in the north lobe is parallel to the axis of the lobe in its interior, and circumferential at the northern and western edges.

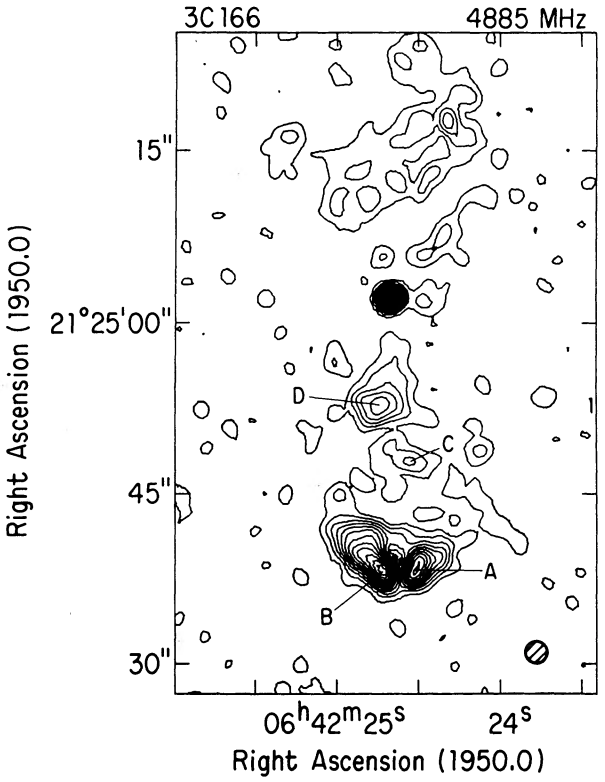

FIG. 3. Map of polarized intensity $(Q^2 + U^2)^{1/2}$ at 4.9 GHz. There are 19 evenly spaced contours beginning at 5% of the peak polarized intensity, which is 5.00 mJy/beam. The restoring beam is 1.6" FWHM. The south lobe features discussed in the text are indicated.

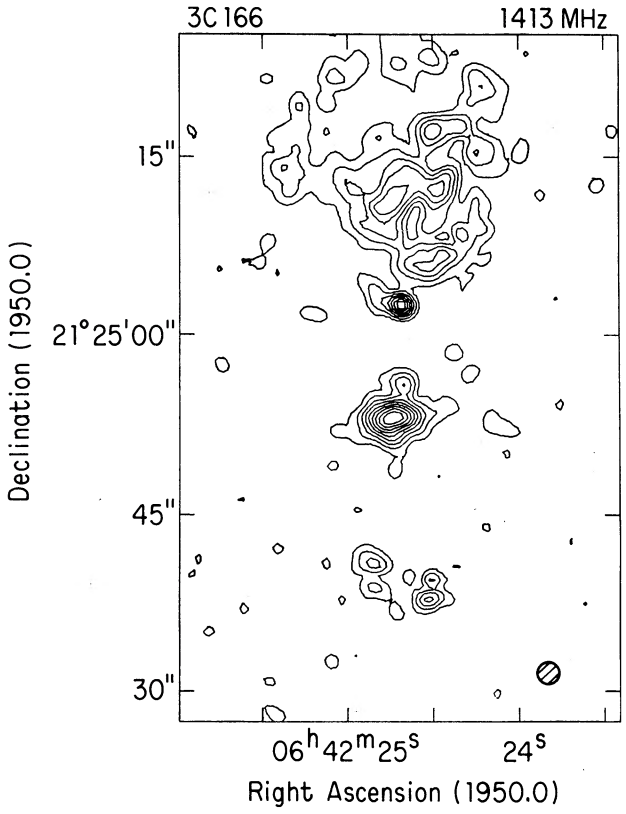

FIG. 4. Map of polarized intensity $(Q^2 + U^2)^{1/2}$ at 1.4 GHz. There are nine evenly spaced contours beginning at 10% of the peak polarized intensity, which is 4.54 mJy/beam. The restoring beam is 1.6" FWHM.

d) Depolarization

We now discuss the depolarization in the south lobe in more detail. Consider first the variation of the map observables along the locus indicated as slice I in Fig. 7 (which shows the 4.9-GHz total intensity image with a number of slices of interest which will be discussed below). The variations of the 4.9- and 1.4-GHz percentage linear polarizations along slice I are shown in Fig. 8. The top panel gives the 1.4-GHz intensity in mJy per beam area. The central panels show the percentage polarizations $[100\cdot(Q^2 + U^2)^{1/2}/I]$ at 1.4 and 4.9 GHz. The bottom panel gives the 1.4–4.9-GHz spectral index [defined in the sense $S(\nu) \propto \nu^{-\alpha}$]. In the plot of 1.4-GHz percentage polarization, an open circle indicates that the value is consistent with noise, given the Ricean statistics of the polarized intensity. The data shown by open circles are therefore upper limits to the percentage polarization at these positions. Figure 8 shows unambiguous evidence for Faraday depolarization between 1.4 and 4.9 GHz in the south lobe: between 0" and 13" (33 kpc) from the rim of the lobe, the 4.9-GHz percentage polarization ranges from 5% to 15% while at 1.4 GHz the percentage polarization is $\leqslant$2% throughout this entire region.

About 13" from the rim of the lobe, the percentage linear polarization increases markedly at both frequencies, indicating a fairly rapid drop in the Faraday depth. The fact that the 4.9-GHz percentage polarization increases at the same position as that at 1.4 GHz, approaching the theoretical limit of 73% (for a spectral index of 0.8), suggests that the diminished 4.9-GHz polarization in the interval 0"–13" might also be due to Faraday depolarization. Observations at a higher frequency and a higher resolution are needed to determine whether this actually is the case, or whether the low 4.9-GHz polarization is due to disordering of the field near the rim of the south lobe on scales less than that of the VLA beam.

The bottom panel shows that the spectral index increases near the point (13" from the rim) where the percentage linear polarization suddenly increases. We stress that these effects are between six and ten times larger than the uncertainties due to residual zero-level bias in the maps. From Figs. 5 and 6 we see that the region of high spectral index and linear polarization is one where the magnetic field is perpendicular to the source axis. These observations suggest a relationship between a drop in the Faraday depth and the occurrence of enhanced particle energy losses, but it is not clear what physical process might produce such a phenomenon. There is no evidence for a discontinuity in the 1.4-GHz total intensity at this location.

The data in Fig. 8 may be used to measure the Faraday depth in different parts of the source. The fractional linear polarization at a frequency ν of a homogeneous source affected by Faraday depolarization in the pres-

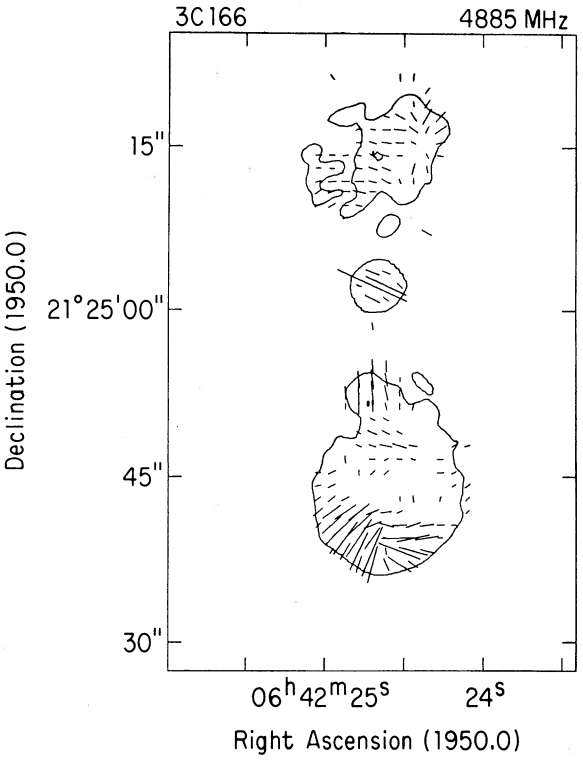

FIG. 5. Plot of electric field vectors at 4.9 GHz, superimposed on the 0.40% contour of the total intensity image from Fig. 1.

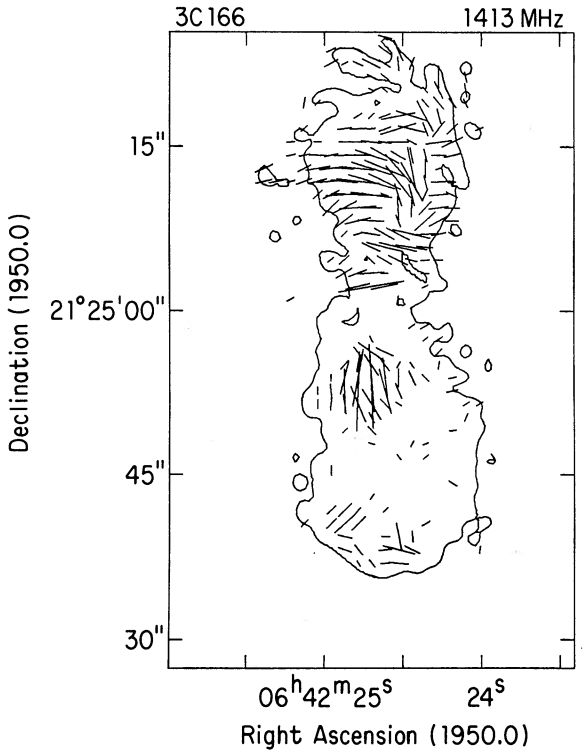

FIG. 6. Plot of electric field vectors at 1.4 GHz, superimposed on the 1% contour of the total intensity image from Fig. 2.

ence of a uniform magnetic field is [Cioffi and Jones 1980, Eq. 4(a)]:

$$m = m_0(2/F_C)|\sin(F_c/2)|. \quad (1)$$

Here m is the observed fractional linear polarization and $m_0 = (3\gamma + 3)/(3\gamma + 7)$ is the intrinsic value of this parameter, i.e., that which would be observed in a well ordered field if no Faraday rotation were occurring. The value of m_0 for an electron spectrum power-law index γ of 2.6, as in 3C 166, is 73%. The quantity F_c is the Faraday depth and is given by $4.7\times10^4\ \nu^{-2}\ n_e B_\parallel L$ for a uniform source, where all quantities are in cgs units. The variables have their usual physical significance.

Equation (1) displays damped oscillation of the fractional polarization when $F_c \geqslant 2\pi$. These oscillations are an artifact of the model used to derive Eq. (1), i.e., a uniform source with a sharp edge. For real, tapered sources, the fractional polarization would approach zero in a monotonic manner which depended on the functional form of the tapering. As this functional form is unknown, we have used Eq. (1) in the range $0 \leqslant F_c \leqslant 6$, where oscillations do not occur and it is not too sensitive to the precise form of the source.

Returning to Fig. 8, we notice that throughout much of the first 12" (30 kpc) of the slice, the mean ratio of 4.9- to 1.4-GHz fractional polarizations is > 5, with values frequently > 10. This implies a lower limit to the 1.4-GHz Faraday depth of at least 5. Most of these values are lower limits since, as mentioned above, most of the 1.4-GHz polarization measurements are consistent with the Ricean noise alone. About 12" (30 kpc) from the rim of the lobe, where the fractional polarization rises at both frequencies, the ratio of 4.9- to 1.4-GHz fractional polarizations is about 1.5, indicating a 1.4-GHz Faraday depth of about 3. A uniform source with this Faraday depth would have a position angle difference between 1.4 and 4.9 GHz of about 40 deg, considerably greater than the < 10 deg observed at this point. This part of the source is probably significantly more complex than is assumed in the uniform model; the effect could result from part of the source lying in front of a heavily depolarizing screen, i.e., if the depolarizing medium lay along the source axis so that part of the lobe emission is behind it and part in front.

This feature could also be interpreted in the context of the pseudorandom field model of extragalactic sources proposed by Laing (1981b). Laing suggests that shearing or compression of initially disordered fields results in a pseudorandom field confined to a plane. The observed degree of linear polarization will then be a strong function of the angle between this plane and the line of sight (being high if the plane contains the line of sight and low when the plane is perpendicular to the line of sight). Laing notes that if thermal matter is introduced in such a model, depolarization can occur without rotation if the scale of the irregularities is smaller than the beam of the telescope. This would be consistent with our observations of feature *D*. Furthermore, the structure of the

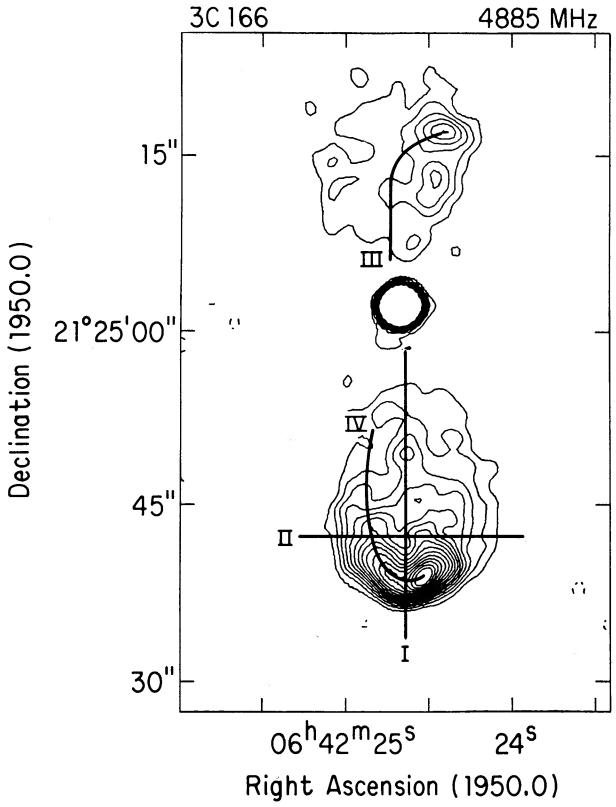

FIG. 7. 4.9-GHz map showing location of four slices along which map observables were examined in detail (see text, Sec. III).

TABLE II. Physical parameters.

Feature	$m_{4.9}$	$m_{1.4}$	F_c(20 cm)	$n_e B_\parallel$	B_{eq} (G)	n_e (cm^{-3})
A	0.13	~0.02	~5.5	$\sim 9.3\times10^{-9}$	4×10^{-5}	$\sim 2\times10^{-4}$
B	0.23	~0.01	~6	$\sim 1.0\times10^{-8}$	4×10^{-5}	$\sim 3\times10^{-4}$
C	0.20	≤0.025	>5.5	$>2.5\times10^{-9}$	2×10^{-5}	$>1\times10^{-4}$
D	0.52	0.39	~2.5	1.1×10^{-9}	2×10^{-5}	$\sim 5\times10^{-5}$
NHS	0.08	0.08	<1.5	$<2\times10^{-5}$	3×10^{-5}	$<7\times10^{-5}$
NL	0.18[a]	0.22[a]	<1.5	$<6\times10^{-10}$	2×10^{-5}	$<3\times10^{-5}$

[a] These measurements possess errors of about 0.03.

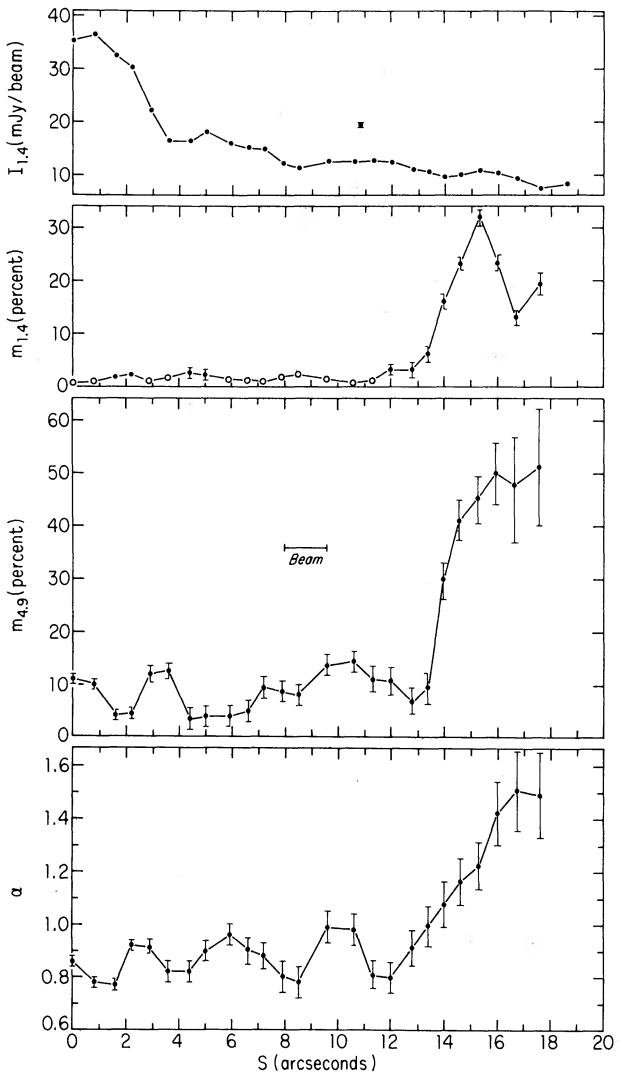

FIG. 8. Variation of map observables along the axis of the south lobe (slice I of Fig. 7). The top panel shows the 1.4-GHz intensity. A typical uncertainty is shown by the error bar. The central panels show the percentage linear polarization at 1.4 (upper) and 4.9 GHz (lower). Closed circles with error bars denote measurements; open circles denote upper limits. The bottom panel shows the 1.4-to 4.9-GHz spectral index.

polarized emission from the south lobe (Fig. 3), with a lack of polarized emission at the center of the lobe, is consistent with a spherical or cylindrical geometry containing a layered magnetic field of the kind described by Laing.

In contrast to these phenomena in the south lobe, the north lobe shows no sign of systematic Faraday depolarization. Figure 9 shows the variation of 1.4-GHz intensity, 1.4-GHz fractional polarization, and 4.9-GHz fractional polarization along a slice (marked as slice III in Fig. 7) parallel to the projected magnetic field. Note the very similar behavior in the fractional polarizations at the two frequencies. Ignoring apparently frequency-specific features which are close to the observational errors and are probably artifacts, we see that the fractional polarization at both frequencies begins at about 10%, rises to 20%–25% between 4″ and 9″ (10 and 23 kpc) from the start of the slice, and thereafter decreases. The mean value of the 1.4 to 4.9-GHz fractional polarization ratio on this slice is 1.03 with a standard deviation of 0.25. Accordingly, the 1.4-GHz Faraday depth is almost certainly less than 2. At both frequencies, the mean fractional polarization along this slice is about 0.18.

e) Physical Parameters

Continuous mapping of the Faraday depth through the source is not possible, because of the low fractional polarizations over most of the map at both 1.4 and 4.9 GHz, and the resulting uncertainties in the polarization ratios. We therefore concentrate on four areas of the south lobe where the 4.9-GHz polarized intensities are well above the noise, as well as on two areas in the north lobe. The south lobe areas are labeled *A*, *B*, *C*, and *D* in Fig. 3. The north lobe areas are the more prominent brightness maximum and the geometrical center of the lobe.

Table II presents the derived physical parameters. Column 1 identifies the feature—NHS for the maximum of the north lobe and NL for its center. Columns 2 and 3 give the 4.9- and 1.4-GHz fractional polarizations, respectively. The minimum 1.4-GHz Faraday depth consistent with the fractional polarizations is listed in column 4.

Column 5 gives the path-averaged values of $n_e B_\parallel$, calculated from the measured Faraday depth using as the

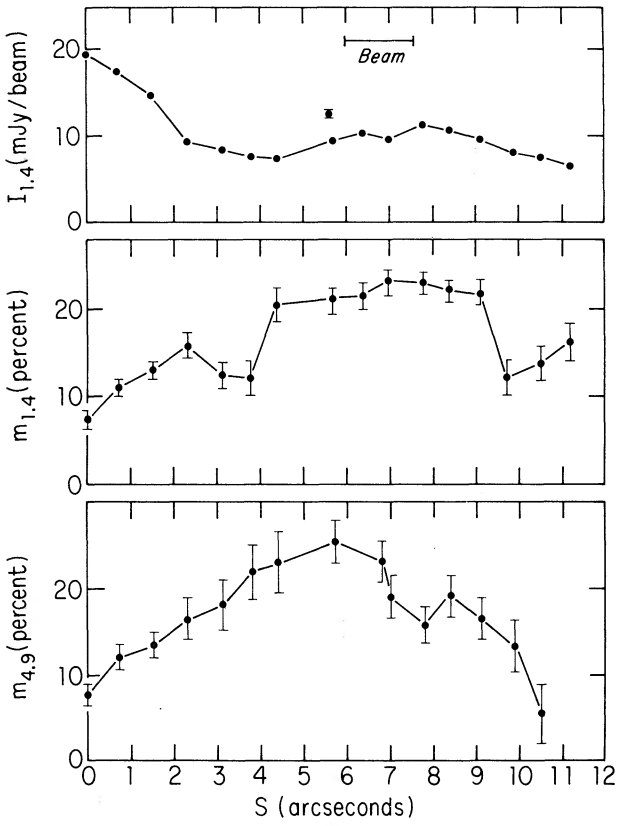

FIG. 9. Variation of map observables along a slice following the magnetic field in the north lobe (slice III). The top panel shows the 1.4-GHz intensity. The lower panels show the 1.4-and 4.9-GHz percentage linear polarizations. Note the absence of a measurable Faraday depth.

line-of-sight path length the transverse diameter of the feature obtained from the maps. Column 6 lists the equipartition magnetic field, calculated with the assumption that the electron spectrum is a power law above 10 MeV and that equal energies reside in relativistic protons and electrons. Column 7 estimates the electron density, approximating $B_{\|}$ in column 5 by the equipartition magnetic field. We remind the reader that these numbers will not be physically meaningful unless the magnetic field in the source is close to the equipartition value and the thermal plasma and magnetic field are both uniform and cospatial. These electron densities should therefore be thought of only as order-of-magnitude estimates. Note that the electron densities for the north lobe are less than those in analogous regions of the south lobe.

IV. DISCUSSION

a) Comments on Polarization and Structure

In the preceding section, we saw that the south lobe of 3C 166 shows evidence of substantial Faraday depolarization, while the north lobe has an immeasurably small Faraday depth. Figures 1 and 2 also show clear morphological differences between the two lobes. The south lobe is more luminous, has an intense outermost rim, and a bright hot spot at the extremity of the lobe. The north lobe, on the other hand, is more diffuse with feeble brightness maxima in its interior.

Is this apparent association between Faraday depth and morphology significant, in the sense of being a general property of the more luminous double sources? Unfortunately, there is a shortage of multifrequency polarimetry of such sources with resolutions comparable to that presented here.

VLA maps of 3C 277.3 at 1.4 and 4.9 GHz (Bridle *et al.* 1981; van Breugel *et al.*, in preparation) show that its lobe structure resembles that of 3C 166 in that the north lobe of 3C 277.3 has a prominent hot spot near its outermost edge whereas the south lobe has a more relaxed structure. The north lobe of 3C 277.3 is also heavily depolarized, whereas the south lobe is not. The depolarization in 3C 277.3 is very probably due to thermal material and not to field disordering on the scale of the VLA beam (a) because the field structure appears well resolved (e.g., Bridle *et al.* 1981) and (b) because line-emitting gas has been detected optically in the regions of lowest polarization (Miley *et al.* 1981). Thus, 3C 277.3 exhibits the same relationship between lobe structure and Faraday depth distribution as does 3C 166.

Studies by Burch (1979), Hogbom (1979), Laing (1981a), and van Breugel (1979) present lower-resolution polarimetry of 14 sources at 1.4, 2.7, and 5 GHz. Of these, six (3C 33.1, 3C 35, 3C 47, 3C 223, 3C 300, and 3C 382) are similar to 3C 166 in the sense that one lobe has a prominent hot spot whereas the other does not. Among these six sources, however, there is no correlation between prominence of the hot spots in the lobes and their depolarization properties. The remaining eight sources of the 14 are "classical doubles"; i.e., both lobes have prominent hot spots. A full range of depolarization properties is seen for these sources.

We conclude, despite the limited amount of suitable data, that there is no evidence for a *general* correlation between Faraday depolarization and lobe morphology, i.e., between the distributions of thermal and nonthermal particles in the lobes.

b) Energetic Electron Transport

A model for nondiffusive electron transport in extragalactic radio sources was developed by Spangler (1979) and Spangler and Basart (1981). They posit an anisotropic, field-aligned spectrum of energetic electrons, and show that an equilibrium generally occurs between pitch angle scattering and synchrotron losses. If this mode of electron transport occurs, the volume emissivity will decrease exponentially with distance from the electron injection site and the radio spectral index gradient will be small or zero. Owing to the nature of the model, the electron transport will be parallel to the magnetic field.

Figure 10 plots the 4.9-GHz total intensity and spectral index along slice IV of Fig. 7; the magnetic field is

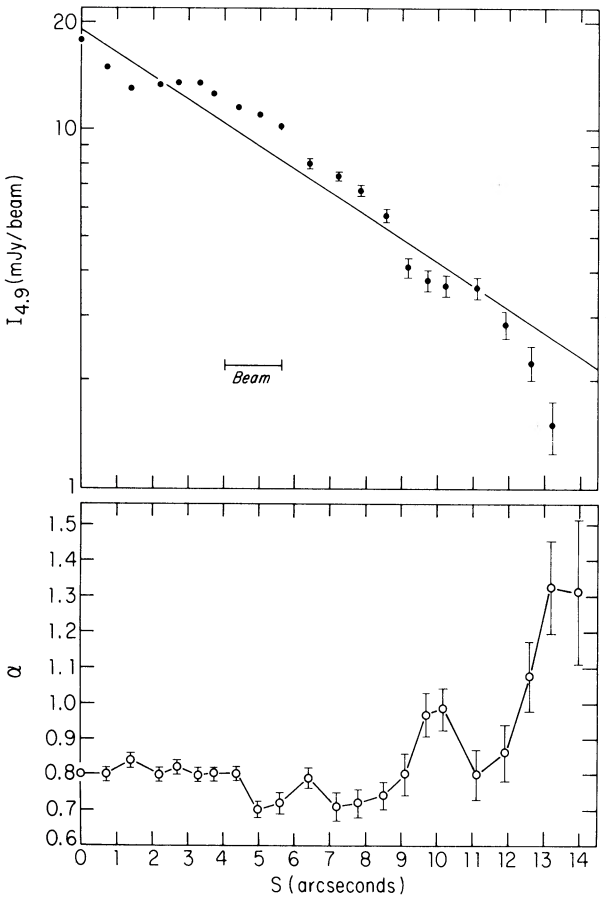

FIG. 10. Variation of map observables along the southeast perimeter of the south lobe (slice IV of Fig. 7). The upper panel shows the 4.9-GHz total intensity; the lower shows the 1.4- to 4.9-GHz spectral index. The slice is approximately parallel to the projected magnetic field at this part of the lobe. It may be seen that for the first 12″ of the slice, the intensity varies according to an exponential law, and there is little or no variation in the spectral index.

parallel to this slice. The decay of the total intensity with distance from the brightest feature (*A*) is approximately exponential with a projected scale length of 6.5″ (16 kpc) over the first 12″ of the slice. There is also little variation in the spectral index. While these observations along slice IV are consistent with the nondiffusive electron transport model, they cannot be regarded as verification of it for several reasons.

First, the conversion from total intensity to volume emissivity requires division by a path length which is an unknown blend of the diffuse lobe and the bright ridge. An attempt to separate the brightness variation on the ridge from that in the underlying lobe by taking profiles transverse to slice IV showed that this separation could not be made unambiguously but also that there was no evidence for a different scale length on the ridge alone.

Second, the quasi-exponential regime cannot be traced over many scale lengths or over a large range in brightness, owing to the finite extent of the lobe and the finite resolution of the data. A projected scale length of $\simeq$15–20 kpc would be compatible with the nondiffusive transport model if the static magnetic field in the region is a few times 10^{-4} G. Appeal to projection effects and to favorable realizations of the model could reduce this requirement to $\simeq 10^{-4}$ G. The equipartition magnetic field estimated in this region of 3C 166 in Table II is thus a factor of 2–10 lower than that required by the transport model.

This disparity of the magnetic field estimates may not compromise the validity of the electron transport model, for two reasons. First, the model *requires* the field energy density to exceed that of the electrons. Second, the equipartition calculations *assume* that the energy resident in relativistic protons equals that in relativistic electrons. There is little reason for this assumption other than that of minimizing the total energy budget of the synchrotron emission. Were we to assume proton-to-electron energy ratios similar to those of galactic cosmic rays or in the solar wind, the equipartition magnetic field would be of the same order as that required by the nondiffusive transport model.

We conclude that the observations of 3C 166 are consistent with, but cannot validate, a nondiffusive model for electron transport away from the hot spot around the limb of the south lobe.

V. CONCLUSIONS

The new VLA observations of 3C 166 at 1.4 and 4.9 GHz have revealed two main features of interest:

(1) The two lobes have strikingly different morphologies and polarization characteristics. The south lobe of 3C 166 has a sharp outermost edge with significantly enhanced brightness, and a hot spot near the extremity of the lobe. This lobe also shows pronounced Faraday depolarization. In contrast, the north lobe is more diffuse, with relatively feeble brightness maxima located in its interior, and a small Faraday depth. Observations of other sources with similar morphologies suggest, however, that the morphological and depolarization properties may not generally be related in this way in other extragalactic sources.

(2) There is a prominent ridge of enhanced intensity extending from the hot spot around the southeast perimeter of the south lobe (slice IV in Fig. 7). The projected magnetic field is parallel to this ridge. Over most of the length of this ridge the intensity declines with distance according to an exponential law, and for the first 12″ there is little change in radio spectral index. The projected intensity scale length is 16 kpc. These observations are consistent with, but not proof of, a mode of nondiffusive electron transport proposed by Spangler (1979) and Spangler and Basart (1981).

The observations reported here raise the general question of what determines the internal structures of the lobes of the extended sources. Although there is a tendency for hot spots at the edges of lobe structures to be more pronounced in more luminous sources (Fanaroff and Riley 1974), radio galaxies such as 3C 166 and 3C

277.3 provide excellent examples of different lobes in the same source having radically different structures and polarization properties. In the context of the "beam" models of continuous energy supply to the hot spots in the lobes (Blandford and Rees 1974), one might be tempted to relate such differences to the energy fluxes provided by the beams—do "hot spots" form when powerful or well collimated beams are entering the lobes, and do more relaxed structures form when the beams are feeble or less well collimated? If so, what governs the beam properties on the two sides of the source? The VLA maps of 3C 166 and 3C 277.3 clearly show that such differences are not related to the presence of detectable radio jets on the two sides of the source—the knotty jet in 3C 277.3 enters the more relaxed lobe, while no jet is detected in either lobe of 3C 166.

We thank Robert Laing for stringent commentary on an earlier draft of this paper.

A. H. B. thanks the NRAO for financial support during a leave of absence from Queen's University of Kingston. This work has been partially supported by an operating grant to A. H. B. from the Natural Sciences and Engineering Research Council of Canada.

REFERENCES

Baars, J. W. M., Genzel, R., Pauliny-Toth, I. I. K., and Witzel, A. (1977). Astron. Astrophys. Suppl. **61**, 99.

Blandford, R. D., and Rees, M. J. (1974). Mon. Not. R. Astron. Soc. **169**, 395.

Bridle, A. H. (1981). In *Extragalactic Radio Sources*, edited by D. S. Heeschen and C. M. Wade (Reidel, Dordrecht).

Bridle, A. H., and Fomalont, E. B. (1978). Astron. J. **83**, 704.

Bridle, A. H., Fomalont, E. B., Palimaka, J. J., and Willis, A. G. (1981). Astrophys. J. **248**, 499.

Burbidge, G. R., and Crowne, A. H. (1979). Astrophys. J. Suppl. **40**, 583.

Burch, S. F. (1979). Mon. Not. R. Astron. Soc. **186**, 519.

Cioffi, D. F., and Jones, T. W. (1980). Astron. J. **85**, 368.

Clark, B. G. (1980). Astron. Astrophys. **89**, 377.

Dreher, J. W. (1981). Astron. J. **86**, 833.

Ekers, R. D., Fanti, R., Lari, C., and Parma, P. (1981). Astron. Astrophys. **101**, 194.

Fanaroff, B. L., and Riley, J. M. (1974). Mon. Not. R. Astron. Soc. **167**, 31P.

Fanti, R., and Parma, P. (1981). In *Optical Jets in Galaxies*, 2nd ESO/ESA Workshop (ESA SP-162), edited by B. Battrick and J. Mort (European Space Agency, Paris), p. 91.

Heeschen, D. S. (1981). In *Telescopes for the 1980s*, edited by G. R. Burbidge and A. Hewitt (Annual Reviews Inc., Palo Alto), p. 1.

Hogbom, J. A. (1974). Astron. Astrophys. Suppl. **15**, 417.

Hogbom, J. A. (1979). Astron. Astrophys. Suppl. **36**, 173.

Kesteven, M. J. L., Bridle, A. H., and Brandie, G. W. (1976). Astron. J. **81**, 919.

Laing, R. A. (1981a). Mon. Not. R. Astron. Soc. **195**, 261.

Laing, R. A. (1981b). Astrophys. J. **248**, 87.

Miley, G. K., Heckman, T. M., Butcher, H. R., and van Breugel, W. J. M. (1981). Astrophys. J. Lett. **247**, L5.

Simard-Normandin, M., and Kronberg, P. P. (1980). Astrophys. J. **242**, 74.

Spangler, S. R. (1979). Astrophys. J. Lett. **232**, L7.

Spangler, S. R., and Cook, D. B. (1980). Astron. J. **85**, 659.

Spangler, S. R., and Basart, J. P. (1981). Astrophys. J. **243**, 1103.

Thompson, A. R., Clark, B. G., Wade, C. M., and Napier, P. J. (1981). Astrophys. J. Suppl. **44**, 151.

van Breugel, W. J. M. (1979). Ph.D. thesis, University of Leiden.

Wyndham, J. D. (1966). Astrophys. J. **144**, 459.